Article

TRANSPARENT PROCESS OPEN ACCESS

EMBO reports

The anti-apoptotic Bcl-2 protein regulates hair follicle stem cell function

Anna Geueke[1,2,†], Giada Mantellato[1,2,†], Florian Kuester[1], Peter Schettina[1], Melanie Nelles[1], Jens Michael Seeger[3], Hamid Kashkar[1,3] & Catherin Niemann[1,2,*]

Abstract

Maintaining the architecture, size and composition of an intact stem cell (SC) compartment is crucial for tissue homeostasis and regeneration throughout life. In mammalian skin, elevated expression of the anti-apoptotic Bcl-2 protein has been reported in hair follicle (HF) bulge SCs (BSCs), but its impact on SC function is unknown. Here, we show that systemic exposure of mice to the Bcl-2 antagonist ABT-199/venetoclax leads to the selective loss of suprabasal BSCs (sbBSCs), thereby disrupting cyclic HF regeneration. RNAseq analysis shows that the pro-apoptotic BH3-only proteins BIM and Bmf are upregulated in sbBSCs, explaining their addiction to Bcl-2 and the marked susceptibility to Bcl-2 antagonism. In line with these observations, conditional knockout of Bcl-2 in mouse epidermis elevates apoptosis in BSCs. In contrast, ectopic Bcl-2 expression blocks apoptosis during HF regression, resulting in the accumulation of quiescent SCs and delaying HF growth in mice. Strikingly, Bcl-2-induced changes in size and composition of the HF bulge accelerate tumour formation. Our study identifies a niche-instructive mechanism of Bcl-2-regulated apoptosis response that is required for SC homeostasis and tissue regeneration, and may suppress carcinogenesis.

Keywords apoptosis; Bcl-2; hair follicle; Lef1; stem cell

Subject Categories Autophagy & Cell Death; Cancer; Stem Cells & Regenerative Medicine

DOI 10.15252/embr.202052301 | Received 18 December 2020 | Revised 8 July 2021 | Accepted 13 July 2021 | Published online 2 August 2021

EMBO Reports (2021) 22: e52301

Introduction

In most tissues, including the mammalian skin, SCs exist in heterogeneous states and localize to specific niches. On a functional level, SC quiescence, self-renewal and differentiation as well as the elimination of damaged SCs have to be tightly regulated to protect the tissue from degeneration or cancerous overgrowth. While it is well established that the niche instructs the activities of tissue-resident stem and progenitor cells (Morrison & Scadden, 2014; Yu *et al*, 2018), it is not sufficiently understood how SCs translate the input of their niche signals into an appropriate and robust molecular response. Epithelial SCs in hair follicles (HFs) are an excellent model to dissect the relevant niche factors and positional cues coordinating SC function. HFs undergo cycles of growth (anagen), regression (catagen) and rest (telogen) (Paus & Cotsarelis, 1999) (Fig EV1A). The cyclic transition from telogen to anagen relies on niche signals, such as Wnt, BMP, Shh and FGF (Kishimoto *et al*, 2000; Rendl *et al*, 2008; Greco *et al*, 2009; Woo *et al*, 2012), and is fuelled by SCs residing in the HF bulge, an anatomical niche found in the lower permanent part of HFs (Lavker *et al*, 2003).

It has been shown that SCs frequently comprise a heterogeneous cell population (Donati & Watt, 2015; Joost *et al*, 2016). How SC heterogeneity is orchestrated on the cellular and molecular levels and how it affects tissue function are currently not well understood. Previous reports showed that slow-cycling label-retaining cells (LRCs) are present in two prominent HFSC populations, basal and suprabasal bulge SCs (bBSCs, sbBSCs) (Cotsarelis *et al*, 1990; Blanpain *et al*, 2004) (Fig EV1B). $CD34^{+}$/$itga6^{low}$ sbBSC and neighbouring $CD34^{+}$/$itga6^{high}$ bBSCs are similar with both SC populations able to self-renew *in vitro* and to generate new HFs when grafted (Blanpain *et al*, 2004). Until now, the molecular mechanisms underlying a position-encoded bulge SC heterogeneity that lead to functional differences in tissue maintenance have not been reported.

The anti-apoptotic Bcl-2 protein is a critical component of the intrinsic (mitochondrial) apoptosis and is highly expressed in HF BSCs (Sotiropoulou *et al*, 2010). The members of the Bcl-2 protein family control mitochondrial outer membrane permeabilization (MOMP) which results in cytochrome c release and triggers the activation of the initiator caspase-9 and executioner caspase-3 and caspase-7 (Taylor *et al*, 2008; Galluzzi *et al*, 2018). In the mammalian skin, Bcl-2 expression has been associated with increased resistance of BSCs to DNA damage-induced cell death (Sotiropoulou *et al*, 2010). In this study, we investigate the physiological function of Bcl-2 for BSCs, the relevance of BSC-specific Bcl-2 regulation and its role for SC-driven skin regeneration and tumour formation.

1 Center for Molecular Medicine Cologne (CMMC), Faculty of Medicine and University Hospital Cologne, University of Cologne, Cologne, Germany
2 Centre of Biochemistry, Faculty of Medicine and University Hospital Cologne, University of Cologne, Cologne, Germany
3 Institute for Medical Microbiology, Immunology and Hygiene (IMMIH), CECAD Research Center, University of Cologne, Faculty of Medicine and University Hospital Cologne, Cologne, Germany
*Corresponding author. Tel: +49 221 47889511; E-mail: cnieman1@uni-koeln.de
†These authors contributed equally to this work

Results

Bcl-2 protects suprabasal bulge SCs

To investigate the role of Bcl-2 in BSC homeostasis, we systemically treated mice with a highly selective Bcl-2 antagonist ABT-199/venetoclax which is currently implemented in cancer therapy (Souers *et al*, 2013; Thijssen & Roberts, 2019). Remarkably, a single i.p. injection of ABT-199 during the resting phase of the hair cycle (postnatal day, Pd50; Fig EV1A) resulted in apoptosis in HF BSCs. Active caspase-3 (aCas3) staining was detected exclusively in the lower part of HFs, including the HF bulge and hair germ (HG), but not in other SCs or tissue locations (Fig 1A and B). More detailed analysis showed that specifically sbBSCs, a subpopulation of BSCs between the new HF and the club hair, were aCas3 positive in ABT-199-treated skin (Figs 1A and EV1B). FACS analysis of BSCs revealed the specific loss of $CD34^{+}/Itga6^{low}$ sbBSCs upon ABT-199 treatment (Fig 1C and D). Quantification showed a dramatic increase (~ 60%) in HFs containing apoptotic BSCs following treatment with ABT-199 compared with controls (Fig 1B). ABT-199 treatment did not increase the number of HF with apoptotic cells in the HG (Fig 1B). Importantly, no $aCas3^{+}$ cells were detected in the dermal papilla (DP), a cluster of specialized stromal fibroblasts that are crucial for the initiation of new HF growth (Fig 1B). Notably, apoptosis of BSCs was also increased in HFs of tail epidermis after ABT-199 treatment, where HFs differ in their architecture (Duverger & Morasso, 2009) (Fig EV1C and D), suggesting that tail BSCs also rely on a Bcl-2-mediated protection mechanism. Different

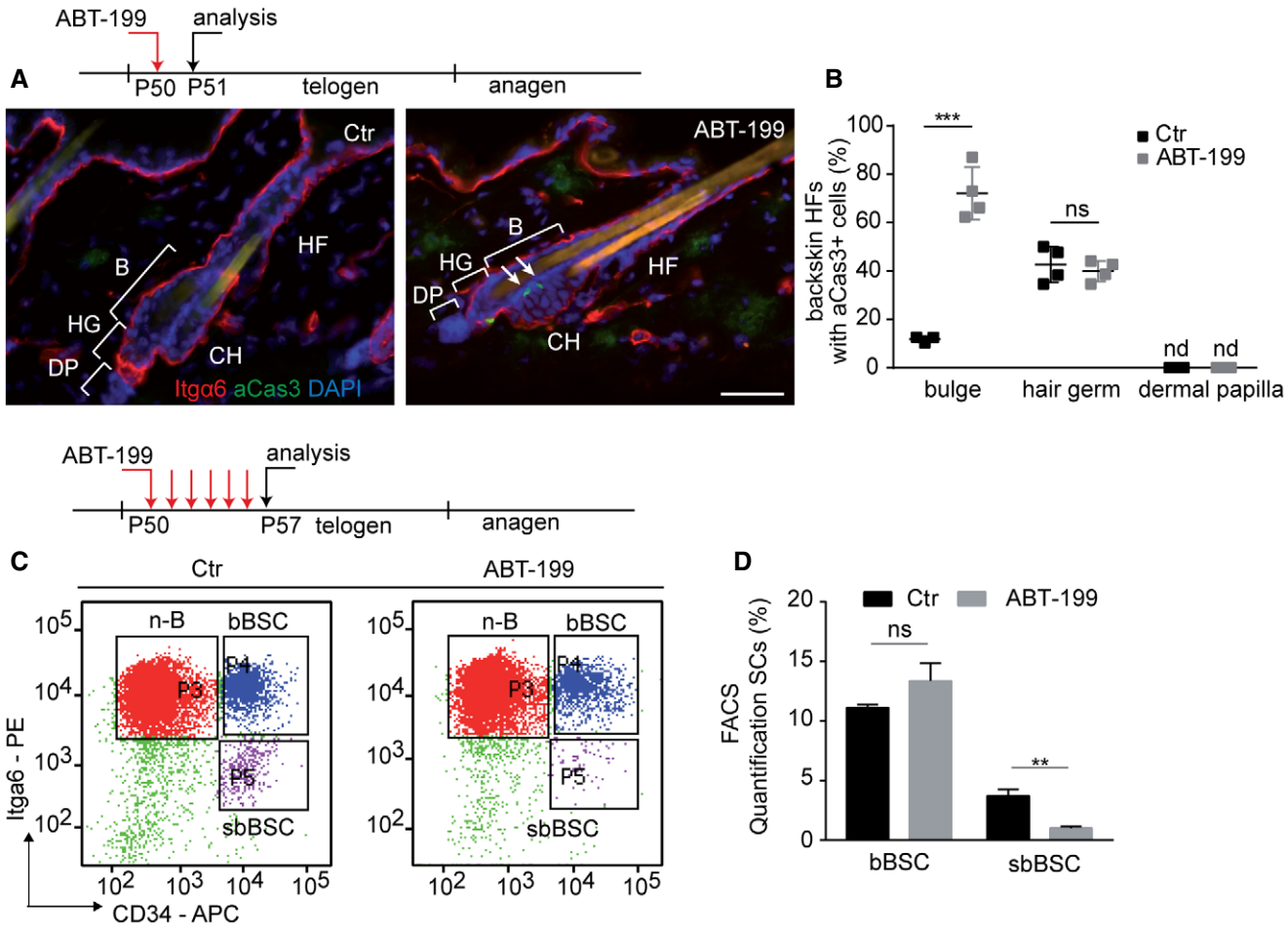

Figure 1. Differential requirement for Bcl-2 preventing suprabasal BSC loss.

A Treatment scheme of experimental timeline and Immunofluorescence staining of telogen back skin hair follicles (HF) for Integrin α6 (Itgα6, red), active caspase-3 (aCas3, green) and DAPI (blue) in control (Ctr) and Bcl-2 inhibitor (ABT-199)-treated mice. B, bulge; CH, club hair; DP, dermal papilla; HF, hair follicle; HG, secondary hair germ. Scale bar, 50 μm.

B Quantification of back skin HF with $aCas3^{+}$ cells in bulge, hair germ and dermal papilla of Ctr and ABT-199-treated mice (n = 4 mice biological replicates; mean ± standard deviation (SD); ***P < 0.001, ns, not significant, two-way ANOVA test). nd, not detected.

C, D Treatment scheme, FACS plot (C) and quantification (D) of keratinocytes stained for CD34 and Itgα6 after 6 days of treatment with vehicle solution (Ctr) or ABT-199 (n = 6 biological replicates; mean ± standard deviation [SD]; **P < 0.01, ns = not significant, two-tailed unpaired Student's t-test). suprabasal (sbBSC, $CD34^{+}/Itg\alpha6^{low}$), basal (bBSC, $CD34^{+}/Itg\alpha6^{high}$) BSCs and n-B (non-bulge epidermal cells). **P < 0.005.

body regions may have developed a general mechanism of safeguarding and maintaining HF SCs. Our findings showed that sbBSCs were distinct from bBSCs in their susceptibility to ABT-199 revealing SC specificity in dependency on anti-apoptotic factors. Next, we tested whether Bcl-2 is differentially expressed in the HF SC populations, which showed that the highest expression of Bcl-2 was in BSCs when compared to isolated Lrig1+ve SCs of the HF junctional zone (JZ) or hair germ (HG) progenitors (Appendix Fig S1B and C). Importantly, the expression of Bcl-2 was particularly high in sbBSCs when compared to bBSCs and non-bulge cells (non-BSCs) (Fig 2A). Further, analysis of Bcl-xL revealed that this anti-apoptotic factor is not differently expressed in sbBSCs compared with bBSCs and non-BSCs, suggesting that Bcl-xL does play a major role in this context (Appendix Fig S1A). Moreover, a number of previous studies already excluded a relevant alteration in platelets, shown to be dependent on Bcl-xL, both in patient and in mice after exposure to ABT-199 (Mason *et al*, 2007; Souers *et al*, 2013; Vandenberg & Cory, 2013; Vogler *et al*, 2013; Debrincat *et al*, 2015; Ganzel *et al*, 2020). We thus conclude that the intrinsically high level of Bcl-2 in $CD34^{+}/Itga6^{low}$ sbBSCs may underlie their specific ABT-199 susceptibility.

Cyclic hair regeneration is regulated by Bcl-2 suprabasal bulge SCs

Given that BSCs drive cyclic hair renewal by initiating a new anagen growth phase (Rompolas & Greco, 2014) (Fig EV1A), we next tested the role of sbBSCs in HF regeneration and investigated the

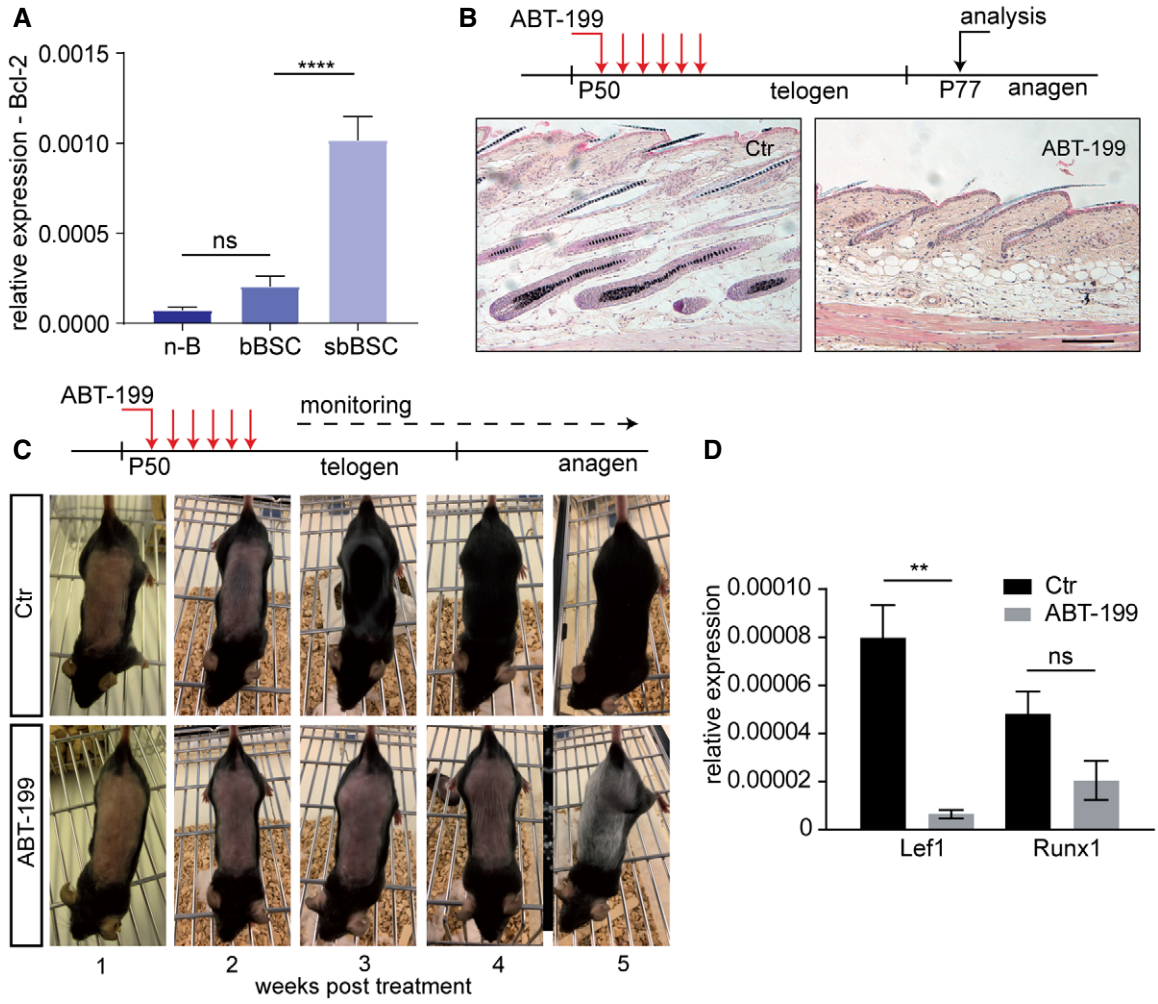

Figure 2. Loss of suprabasal BSCs delays cyclic hair regeneration.

A qRT–PCR for Bcl-2 mRNA expression in sorted n-B (non-Bulge), bBSC (basal BSCs) and sbBSC (suprabasal BSCs; $n = 3$ biological replicates; mean ± standard deviation [SD]; ****$P < 0.0001$, ns=not significant, two-way ANOVA test).

B Treatment scheme of experimental timeline and histology of back skin sections of control (Ctr) and ABT-199-treated mice. Scale bar, 200 μm.

C Treatment scheme and hair-coat recovery monitored for 5 weeks following daily treatment (Pd50–Pd55) with vehicle solution (Ctr) and ABT-199.

D qRT–PCR for mRNA expression of the transcription factors Lef1 and Runx1 in epidermis of ABT-199-treated and control (Ctr) mice at P77 as shown in (B) ($n = 3$ biological replicates; mean ± standard error of mean (SEM); **$P < 0.01$, ns=not significant, two-tailed unpaired Student's *t*-test).

physiological relevance of the sbBSC Bcl-2 dependency. Therefore, we treated mice with ABT-199 during the telogen resting phase to deplete sbBSCs (Pd50) and analysed skin samples during the following anagen phase (Pd77; Figs 2B and EV1B). Depletion of sbBSCs by ABT-199 significantly delayed hair growth for up to 3 weeks (Fig 2C; Appendix Fig S2A). In contrast to the normal hair growth observed in control mice at 3 weeks after treatment, ABT-199 treatment efficiently blocked telogen to anagen transition in the back skin and tail epidermis (Fig 2B; Appendix Fig S2B). This observation was supported by reduced expression of Lef1 and Runx1, transcription factors associated with hair growth, in mice treated with ABT-199 (Fig 2D) (Merrill *et al*, 2001; Hoi *et al*, 2010). Interestingly, ABT-199 treatment also resulted in hair greying (Fig 2C). This observation is in line with previous data from Bcl-2 knockout mouse models demonstrating the importance of Bcl-2 for melanocyte survival and skin pigmentation and most likely occurs independent from sbBSC loss (Yamamura *et al*, 1996; Mak *et al*, 2006). In this context, we detected a high number of melanocytes as shown by immunofluorescence staining for Trp2 (Fig EV1E) indicating that cell death detected in the HG may reflect apoptotic melanocytes. Together our data indicated that sbBSCs, and thus the composition and architecture of the BSC compartment, are important for anagen initiation and cyclic hair regeneration. The results also suggested that Bcl-2 dependency of a SC subpopulation is crucial for tissue homeostasis.

To examine whether the Bcl-2 dependency of BSCs changes during the different stages of the hair cycle, mice were treated with ABT-199 in anagen (Pd70) and analysed during the same anagen phase 1 week later (Pd77; Fig EV1A, Appendix Fig S2C). Histological analysis of skin tissue sections revealed that progression through anagen was not affected. Although the expression of transcription factors Lef1 and Runx1 showed some variability between individual mice during the anagen phase after ABT-199 treatment, it was not significant (Appendix Fig S2D). In addition, ABT-199 treatment during anagen did not result in increased apoptosis (Appendix Fig S2E). Given that HF morphology, including the sbBSC compartment, is dramatically re-modelled during anagen (Hsu *et al*, 2011), the data support Bcl-2-mediated protection of sbBSCs during telogen but not anagen.

To investigate whether Bcl-2 genetic deletion from the epidermis affects BSCs, we generated Bcl-2 epidermal knockout mice (Bcl-2^{EKO}) by crossing K14Cre (Hafner *et al*, 2004) with Bcl-$2^{fl/fl}$ animals (Thorp *et al*, 2009). Similar to the ABT-199 experiments, apoptotic cells were increased in the HF bulge and the number of HFs showing aCas3^{+} BSCs rose from 10 to 60% in tail skin, while no change in the number of tail skin HFs with aCas3^{+} HG cells was detected (Appendix Fig S3A and B). However, no depletion of sbBSCs was detected in Bcl-2^{EKO} mice (Appendix Fig S3C). This suggested that the acute inhibition of Bcl-2 by ABT-199 treatment induces a more severe sbBSC response than genetically and developmentally removing Bcl-2, which most likely allowed adaption and rewiring of the network to compensate for its absence. Alternatively, although established as highly selective Bcl-2 inhibitor (Souers *et al*, 2013), ABT-199 treatment may have interfered with other Bcl-2-family members or other anti-apoptotic proteins expressed by sbBSCs. Collectively, our data showed an anti-apoptotic Bcl-2 dependency of sbBSCs and identified an important function for Bcl-2 in HF homeostasis and regeneration.

Suprabasal bulge SCs may be prone to detachment-induced apoptosis

To investigate sbBSCs Bcl-2 dependency compared to their neighbouring bBSCs and to dissect the cell-intrinsic properties of the heterogeneous BSCs, we performed RNAseq on FACS sorted CD34^{+}/Itga6^{low} and CD34^{+}/Itga6^{high} BSCs. We focused on the differential regulation of cell death response mechanisms, where gene ontology (GO) and functional classification revealed two biological clusters of interest. The first cluster "positive regulation of apoptosis process" included upregulated pro-apoptotic genes, while the second cluster 'cell adhesion mediated by integrin' included downregulated genes for cell adhesion in sbBSCs (Fig 3A and B). An important cellular process that bridges both functional GO clusters is detachment-induced apoptosis, also known as anoikis (Taddei *et al*, 2012). In particular, expression of Bmf and Bim, two pro-apoptotic and anoikis-associated BH3-only members of the Bcl-2 protein family (Puthalakath *et al*, 2001; Taddei *et al*, 2012), was significantly upregulated in sbBSCs compared to bBSCs by both RNAseq data and qRT–PCR (Fig 3B and C). Our data suggested that the lack of integrin-mediated basal lamina attachment (Fig 3B) in sbBSCs and their expression of pro-apoptotic and anoikis-associated molecules, including Bim and Bmf (Fig 3B and C), may be counter-acted by an upregulation of Bcl-2 (Fig 2A), which protects these cells from undergoing apoptosis to ensure efficient cyclic HF regeneration (Fig EV1F).

Bcl-2 activity controls the size and architecture of the bulge SC compartment

Next, we wanted to know whether Bcl-2 and apoptosis regulation play an instructive role for the composition of the BSC compartment and whether increased Bcl-2 expression affects SC function and cyclic hair regeneration. Therefore, we overexpressed *Bcl-2* in the epidermis (Bcl-2^{EOE} mice) by crossing K14Cre (Hafner *et al*, 2004) with Rosa26$^{LSL.Bcl2.IRES.GFP}$ mice (Knittel *et al*, 2016) (Appendix Fig S4A). Bcl-2^{EOE} mice displayed a robust overexpression of *Bcl-2* as shown by mRNA levels (~ 17-fold increase in expression; Appendix Fig S4B) and BCL-2 and GFP levels as seen in epidermal keratinocytes, including the HF and IFE (Appendix Fig S4C–E).

Next, we analysed whether Bcl-2 overexpression affected HF architecture and homeostasis in adult mice. Strikingly, the bulge area was enlarged and filled with densely packed keratinocytes in Bcl-2^{EOE} HFs (Fig 4A and B; Appendix Fig S6A). Based on our results showing particular high Bcl-2 expression in sbBSCs (Fig 2A), we wondered whether Bcl-2 plays an instructive role by regulating the composition of the BSC compartment. However, no changes in the CD34^{+}/Itga6^{high} and CD34^{+}/Itga6^{low} BSC populations were detected in 8-week-old Bcl-2^{EOE} mice, indicating that Bcl-2 expression does not affect the composition of the BSC pool, including the number of bBSCs and sbBSCs (Fig 4C).

More detailed analysis of known BSC marker, including Keratin 15, Sox 9 and Nfatc1 (Liu *et al*, 2003; Vidal *et al*, 2005; Horsley *et al*, 2008; Nowak *et al*, 2008), revealed that these SC markers were all expressed similar to controls within the enlarged HF bulge (Fig EV2A–C). In addition, we did not observe cyst formation or abnormal expression of hair keratins in HFs of Bcl-2^{EOE} mice (Appendix Fig S5A–D), indicating that differentiated hair keratinocytes did not contribute to the enlarged bulge. In order to check

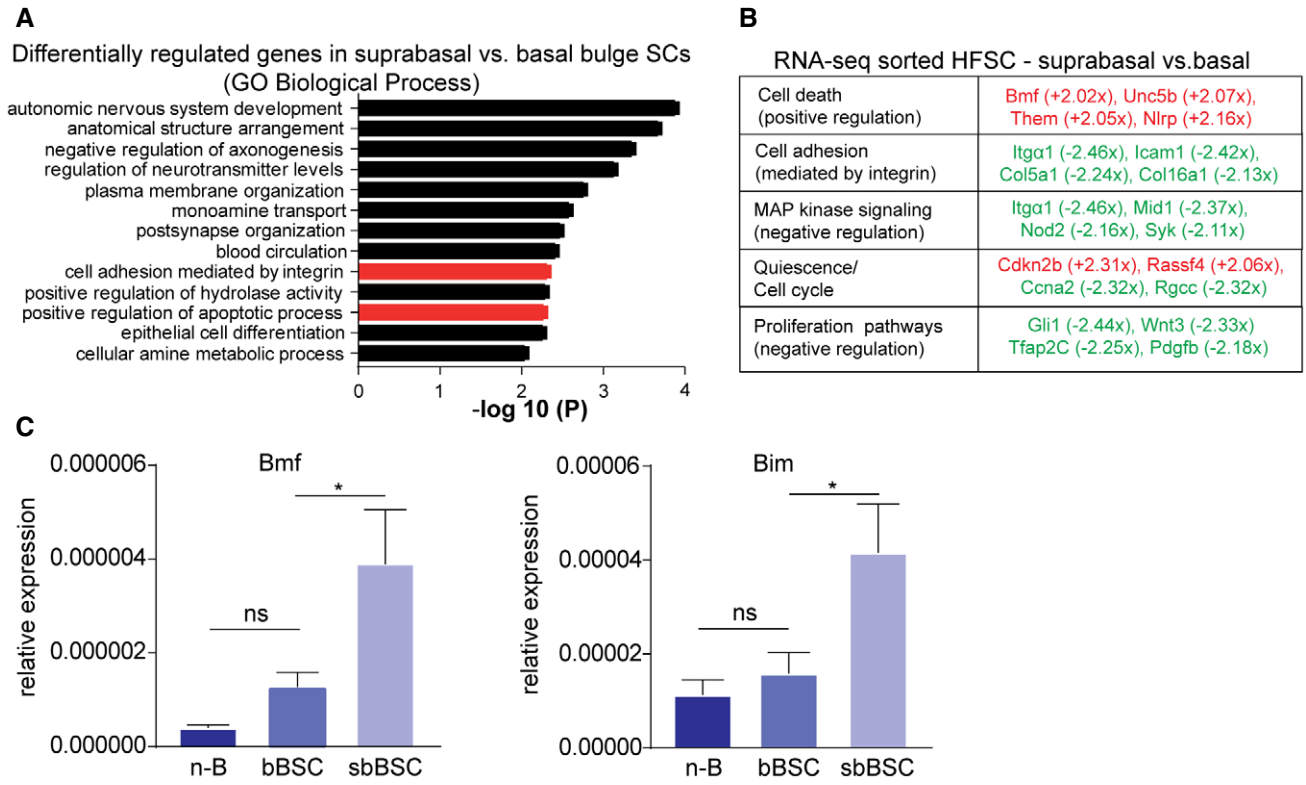

Figure 3. Suprabasal BSCs are prone to detachment-induced apoptosis.

A GO classification of differentially regulated genes in P50 suprabasal BSCs ($CD34^+/Itg\alpha6^{low}$) compared with basal BSCs ($CD34^+/Itg\alpha6^{high}$) clustered for biological process (clustering and statistical analysis done with Metascape, according to Zhou *et al*, 2019). Columns of interest in red.

B Functional classification of selected differentially expressed genes in sorted suprabasal BSC vs basal BSC after RNAseq analysis (red: upregulated genes, green: downregulated genes; fold change > 2, $P < 0.05$; statistical analysis done according to Wagle *et al*, 2015).

C qRT–PCR for mRNA expression of the anoikis-related markers Bim and Bmf in sorted n-B (non-bulge), bBSC (basal BSCs) and sbBSC (suprabasal BSCs; $n = 3$ biological replicates; mean ± standard error of mean [SEM]; $^*P < 0.05$, ns, not significant, two-way ANOVA test).

whether these cells belonged to the HG, immunostaining for P-cadherin was performed (Müller-Röver *et al*, 1999). The localization of the HG below the HF bulge was not altered; however, the increased BSC compartment affected the shape and architecture of the HG highlighting the cellular crosstalk between the two HF compartments (Fig EV2D). Further analysis of RNA expression of P-cadherin, Keratin14 and Lgr6 revealed that these cell populations were rather decreased in Bcl-2^{EOE} mice and most likely did not contribute to the enlarged HF bulge area (Fig EV2E). Next, we investigated whether abnormal SC proliferation may be contributing to the enlarged HF bulge area in Bcl-2^{EOE} mice. Importantly, no change in BrdU incorporation (one pulse BrdU and 1 h chase) was observed between Bcl-2^{EOE} mice and control littermates at P60 (Fig 4D and E), indicating that increased proliferation might not contribute to the enlarged HF bulge area in Bcl-2^{EOE} mice.

Bcl-2 overexpression blocks physiological apoptosis that is required for cyclic hair follicle regeneration

Given that apoptosis is a physiological process during the regression phase (catagen) (Lindner *et al*, 1997; Mesa *et al*, 2015a), we hypothesized that the Bcl-2^{EOE} phenotype was linked to impaired apoptosis during catagen. Therefore, we first focused on the process of HF transition through catagen (Fig EV1A). Strikingly, the column of keratinocytes forming the retracting epithelial strand was wider in Bcl-2^{EOE} mice, suggesting that apoptosis was indeed impaired as expected (Fig 5A and B). Consistently, $aCas3^+$ cells were not detectable in Bcl-2^{EOE} mice compared to controls (Fig 5C and D and Appendix Fig S6B and C). Remarkably, HFs eventually retract in Bcl-2^{EOE} mice despite an efficient block in apoptosis, where the length of the retracting strand was not affected in these mice (Fig 5B). Thus, our data showed that Bcl-2 overexpression throughout the epidermis interfered with HF regression by promoting cell survival in the retracting epithelial strand, thereby increasing the HF bulge area and altering HG architecture.

The abnormal architecture of HF bulge area in Bcl-2^{EOE} mice prompted us to test whether this abnormality affected SC activation at the beginning of a new hair growth phase. Assessing cyclic HF regeneration revealed that the entry into the anagen phase was significantly delayed in Bcl-2^{EOE} mice (Fig 5E). This correlated with increased expression of Bmp6, FGF 18, NFATC1 and FOXP1, proteins that are associated with the quiescent state of BSC (Blanpain *et al*, 2004; Kimura-Ueki *et al*, 2012; Leishman *et al*, 2013) in Bcl-2^{EOE} mice (Figs 5F and G, and EV3A). In addition, Lef1 and

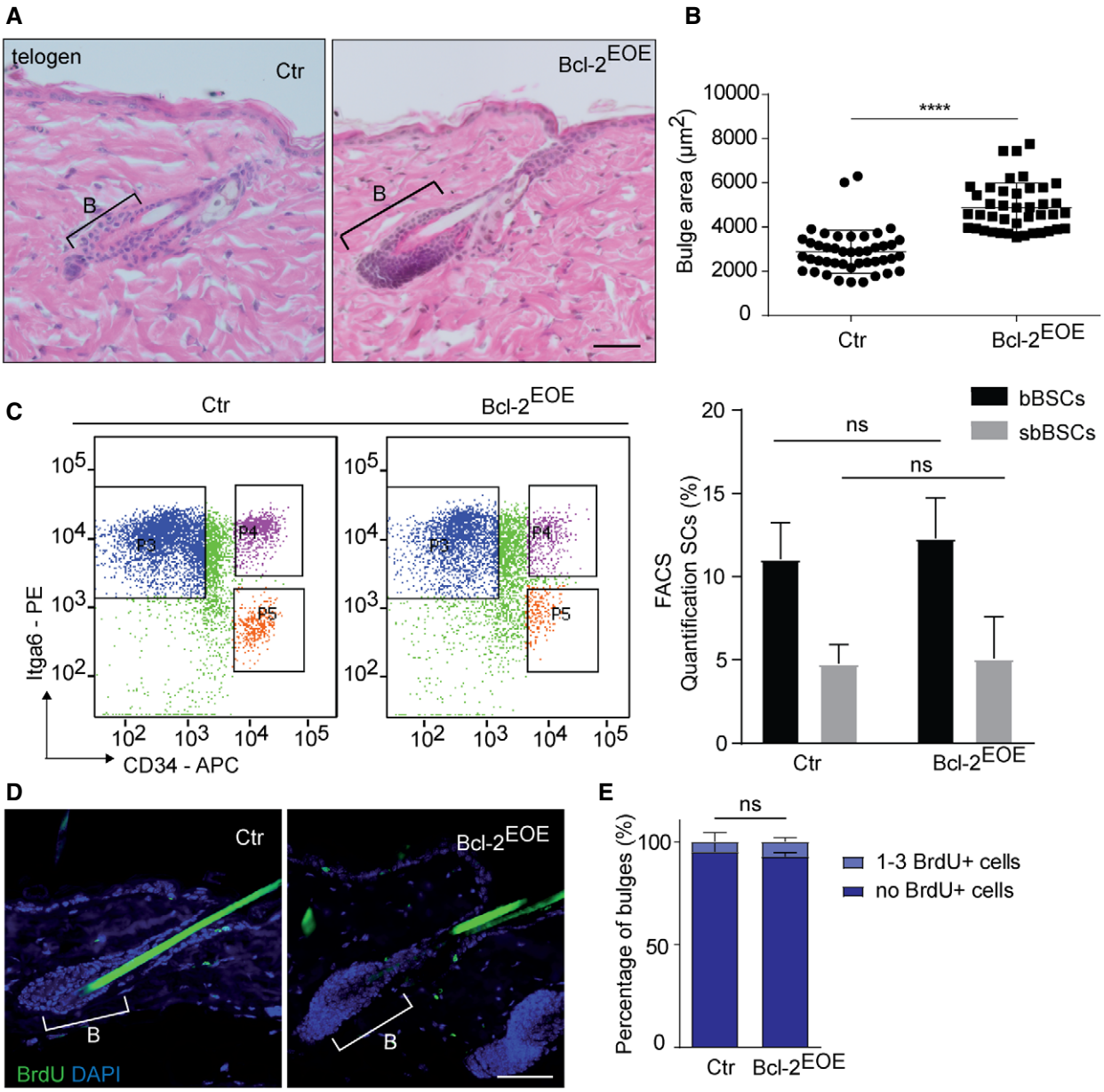

Figure 4. Bcl-2 expression regulates size and architecture of SC compartment and delays hair-coat recovery.

A Histology of telogen back skin HF of Ctr and Bcl-2^{EOE} mice (P60). B, bulge. Scale bar, 50 µm.

B Quantification of the bulge area in back skin at P60 (n = 4; multiple measurements/biological replicate; mean ± standard deviation [SD]; ****P < 0.0001, two-tailed unpaired Student's t-test).

C FACS plot and quantification of keratinocytes stained for CD34 and Itgα6 in 8-week-old control (Ctr) and Bcl-2^{EOE} mice (n = 3 biological replicates; mean ± standard deviation [SD]; ns, not significant, two-tailed unpaired Student's t-test). suprabasal (sbBSC, $CD34^+/Itg\alpha6^{low}$), basal (bBSC, $CD34^+/Itg\alpha6^{high}$) BSCs.

D Immunofluorescence staining of telogen back skin HF for BrdU incorporation (1-h pulse, green) and DAPI (blue) in 8-week-old control (Ctr) and Bcl-2^{EOE} mice. Scale bar, 50 µm.

E Quantification of $BrdU^+$ bulge cells of Ctr and Bcl-2^{EOE} mice. (n = 4 biological replicates; mean ± standard deviation [SD]; ns, not significant, two-tailed unpaired Student's t-test).

Runx2 expression was reduced in Bcl-2^{EOE} epidermis (Fig EV3B), and proliferation of HG cells, as examined by 1 h BrdU pulse, was not initiated in Bcl-2^{EOE} mice when compared to control mice (Fig EV3C). Taken together, our data suggested that the proper regulation of cell death during catagen is required for physiological HF regeneration and SC niche identity during telogen. Our findings also revealed that although a Bcl-2-mediated block of apoptosis allows upwards movement of the retracting strand during catagen, the execution of a normal hair cycle, including anagen phase induction, is defective (Fig EV3D).

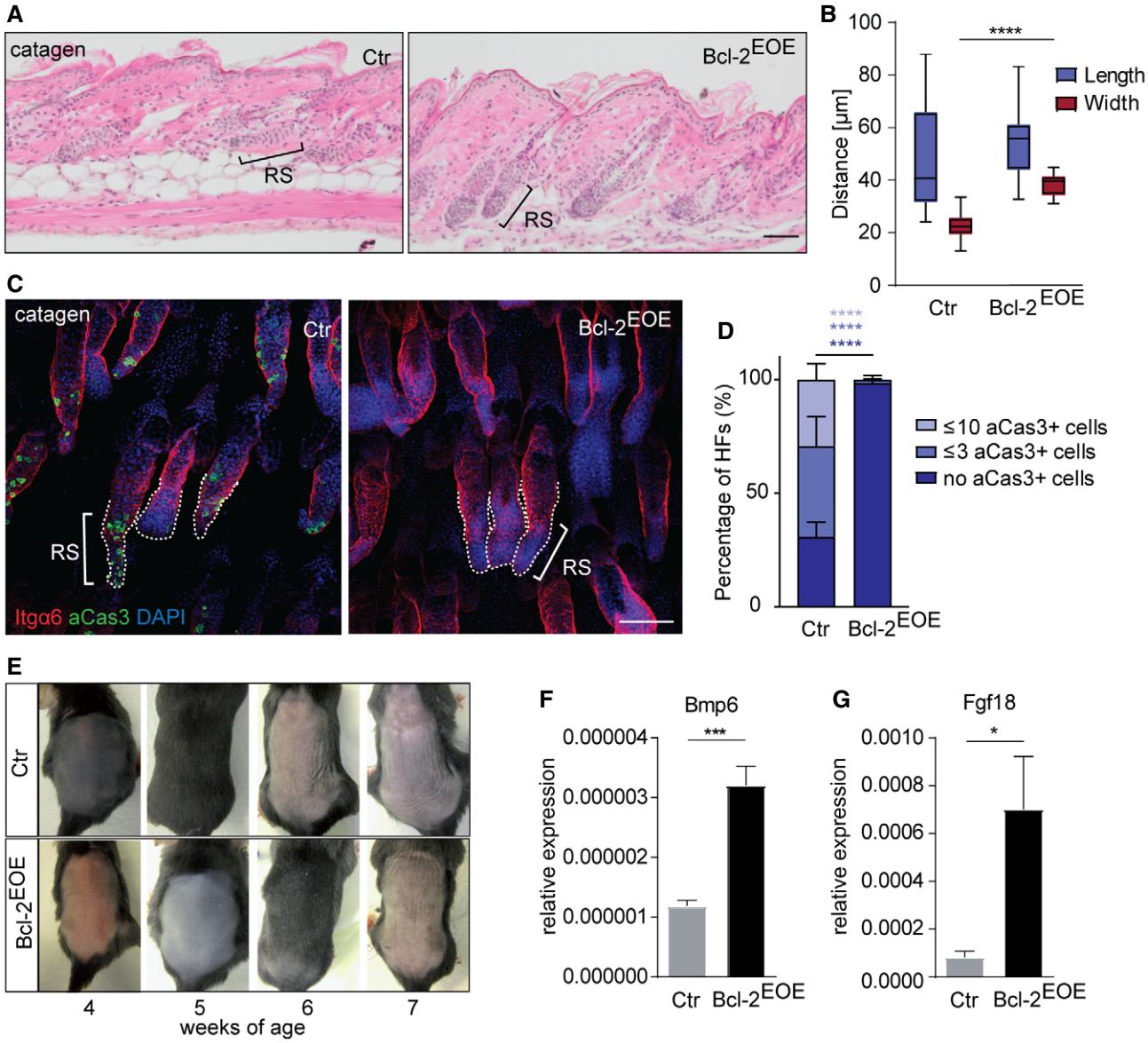

Figure 5. Bcl-2 blocks apoptosis during catagen of the hair follicle cycle.

A Histology of P19 catagen back skin HF of control (Ctr) and Bcl-2^{EOE} mice. RS: retracting strand, Scale bar, 50 µm.

B Analysis of length and width of retracting strands of control (Ctr) and Bcl-2^{EOE} mice (n = 4; multiple measurements/biological replicate; whiskers: min and max; boxes: median ± first and third quartile; ****P < 0.0001, two-tailed unpaired Student's t-test).

C Itgα6 and aCas3 immunofluorescence staining of catagen tail skin HF of control (Ctr) and Bcl-2^{EOE} mice (n = 4 biological replicates). Dashed lines: retracting strands. Scale bar, 100 µm.

D Quantification of $aCas3^{+}$ cells in the RS of P19 Ctr and Bcl-2^{EOE} mice (n = 4 biological replicates; mean ± standard deviation [SD]; ****P < 0.0001, two-tailed unpaired Student's t-test). HF, hair follicle.

E Hair-coat recovery in Ctr and Bcl-2^{EOE} mice following depilation (n = 3 biological replicates).

F, G qRT–PCR for mRNA expression of the quiescence-related markers Bmp6 (F) and Fgf18 (G) in epidermis of control (Ctr) and Bcl-2^{EOE} mice (P27), (n = 4 biological replicates; mean ± standard error of mean [SEM]; *P < 0.05, ***P < 0.001, two-tailed unpaired Student's t-test).

Bcl-2 promotes SC-driven tumour initiation

Based on our data that Bcl-2 overexpression blocks apoptosis during HF regression leading to an enlarged bulge area, we next investigated the pathophysiological consequences of increased Bcl-2 activity in the epidermis including HF SCs. More precisely, we addressed the impact of Bcl-2 overexpression on epidermal tumour formation using the K15ΔNLef1 mice, which express a dominant-negative mutated form of the transcription factor Lef1 (lacking N-terminal β-catenin binding site) specifically in BSCs leading to cancer formation (Petersson *et al*, 2015). Of note and in contrast to wild-type animals, treatment of K15ΔNLef1 mice with a single

sub-threshold dose of the carcinogen DMBA induced skin tumours in high frequency (Petersson *et al*, 2015). Interestingly, BSCs frequently undergo p53-independent apoptosis and Bcl-2 mRNA and BCL-2 protein expression was reduced in K15ΔNLef1 mice compared to controls (Petersson *et al*, 2015) (Figs 6A, and EV4A). To investigate how Bcl-2 regulation affected BSC-driven tumour formation, we generated K15ΔNLef1/Bcl-2^{EOE} mice (Figs 6A, and EV4A and B). In line with previous data (Petersson *et al*, 2015), we detected increased apoptosis in K15ΔNLef1 mice (Fig 6B and C), which was efficiently blocked in K15ΔNLef1/Bcl-2^{EOE} mice (Fig 6B and C). In addition, we observed reduced proliferation of the BSCs in K15ΔNLef1/Bcl-2^{EOE} mice when compared to

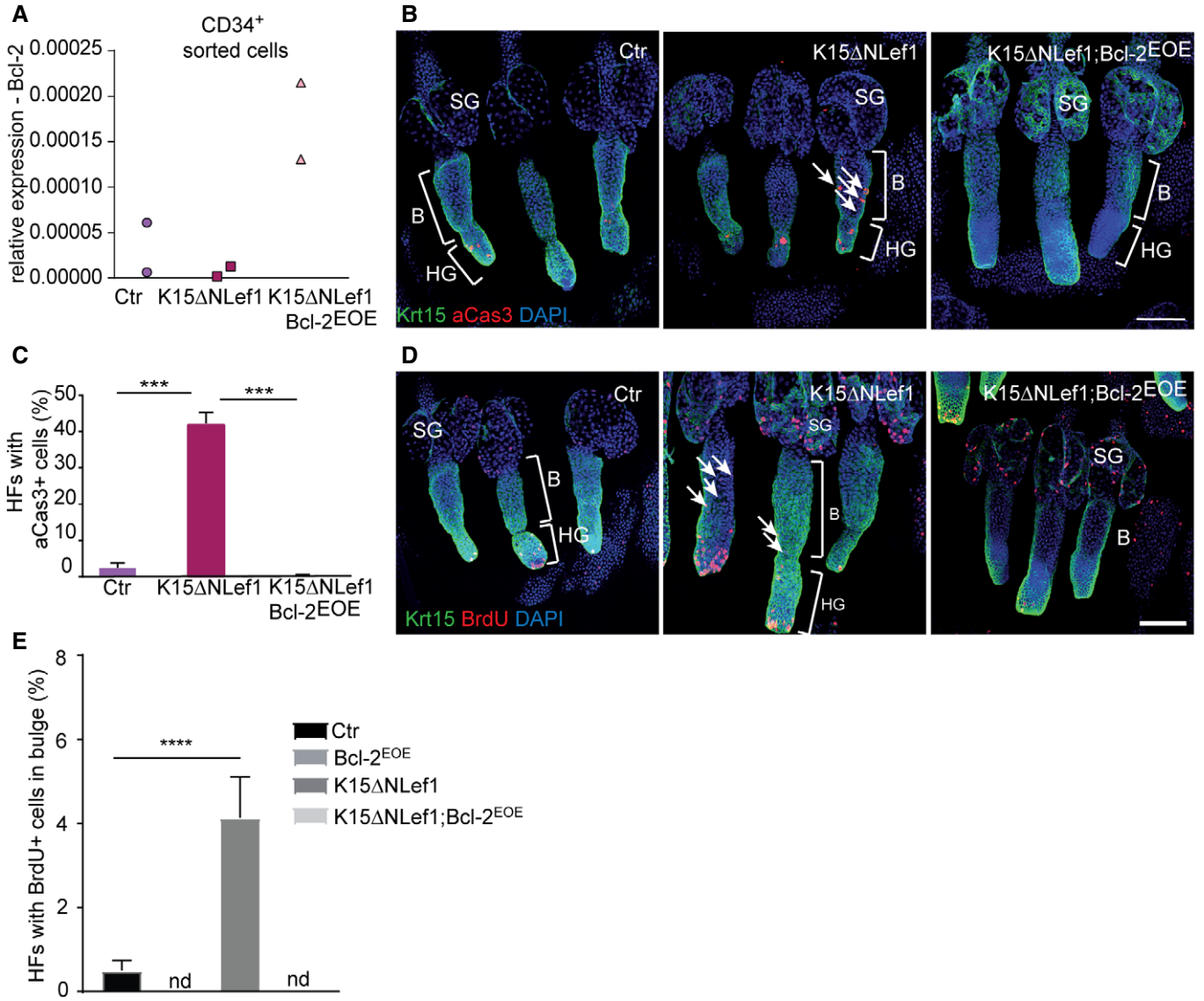

Figure 6. Bcl-2 overexpression blocks BSC apoptosis and proliferation in K15ΔNLef1 mice.

A qRT–PCR for Bcl-2 mRNA expression in sorted (CD34^{+}) BSCs of control (Ctr), K15ΔNLef1 and K15ΔNLef1;Bcl-2^{EOE} mice (n = 2 biological replicates).

B Immunofluorescence staining of epidermal tail whole mounts of control (Ctr), K15ΔNLef1 and K15ΔNLef1;Bcl-2^{EOE} mice, stained for keratin 15 (Krt15, green), activated caspase-3 (aCas3, red) and DAPI (blue). Note increased number of aCas^{+} cells in the bulge of K15ΔNLef1 mice (arrows). B: bulge, HG: secondary hair germ, SG: sebaceous gland. Scale bar, 100 μm.

C Quantification of hair follicles (HF) with activated caspase-3 (aCas3^{+}), apoptotic cells in control (Ctr), K15ΔNLef1 and K15ΔNLef1;Bcl-2^{EOE} mice (n = 6 biological replicates; mean ± standard deviation [SD]; ***P < 0.001, two-way ANOVA test).

D Immunofluorescence staining of epidermal tail whole mounts of control (Ctr), K15ΔNLef1 and K15ΔNLef1;Bcl-2^{EOE} mice, stained for keratin 15 (Krt15, green), BrdU (1-h pulse, red) and DAPI (blue). Note increased number of BrdU^{+} cells in the bulge of K15ΔNLef1 mice (arrows). B, bulge; HG, secondary hair germ; SG, sebaceous gland. Scale bar, 100 μm.

E Quantification of hair follicles (HF) with BrdU^{+}, proliferating cells in bulge of control (Ctr), Bcl-2^{EOE}, K15ΔNLef1 and K15ΔNLef1;Bcl-2^{EOE} mice (n = 6 biological replicates; mean ± standard deviation [SD]; ****P < 0.0001, multiple t-test comparisons). nd, not detected.

K15ΔNLef1 mice, suggesting that apoptosis-induced proliferation may contribute to propagation of mutated BSCs in K15ΔNLef1 mice (Fig 6D and E).

To investigate tumour initiation, K15ΔNLef1 and K15ΔNLef1/Bcl-2^{EOE} mice were treated with DMBA (Niemann *et al*, 2007; Frances *et al*, 2015; Petersson *et al*, 2015) (Fig 7A). Importantly, Bcl-2 overexpression significantly facilitated tumour formation in K15ΔNLef1/Bcl-2^{EOE} mice (3 weeks post-treatment) compared with K15ΔNLef1 mice (5–7 weeks post-treatment; Fig 7B). Moreover, all of the K15ΔNLef1/Bcl-2^{EOE} mice possessed tumours 5 weeks after DMBA treatment, while in contrast, K15ΔNLef1 mice were just beginning to show signs of lesions (Fig 7B and C). As expected, control mice, including Bcl-2^{EOE} and wild-type mice, did not develop epidermal tumours (Fig 7B and C). Further analysis revealed that the epidermal tumour type and sebaceous differentiation of the tumours was not altered following Bcl-2 expression (Petersson *et al*, 2015) (Figs 7D and EV4C and D). The number of tumours per mouse was slightly increased in K15ΔNLef1/Bcl-2^{EOE} animals, likely because the K15ΔNLef1/Bcl-2^{EOE} mice formed tumours much earlier compared with their K15ΔNLef1 littermates (Fig 7C). In addition, proliferation and apoptosis of keratinocytes within the tumour mass was not altered in K15ΔNLef1/Bcl-2^{EOE} mice when compared to K15ΔNLef1 littermates (Fig EV4E and F). The data support our hypothesis that the BSCs expressing higher levels of Bcl-2 possess a growth advantage due to their enhanced survival and therefore contribute to increased tumour formation.

To directly test for the contribution of BSC-specific Bcl-2 overexpression to the accelerated tumour growth detected in K15ΔNLef1/Bcl-2^{EOE} mice, we generated Bcl-2^{K19OE} mice targeting Bcl-2 specifically to keratin 19-expressing HF bulge cells in the mouse epidermis (Means *et al*, 2008). Therefore, the Bcl-2^{K19OE} and K15ΔNLef1 mouse lines were crossed to generate K15ΔNLef1/Bcl-2^{K19OE} mice

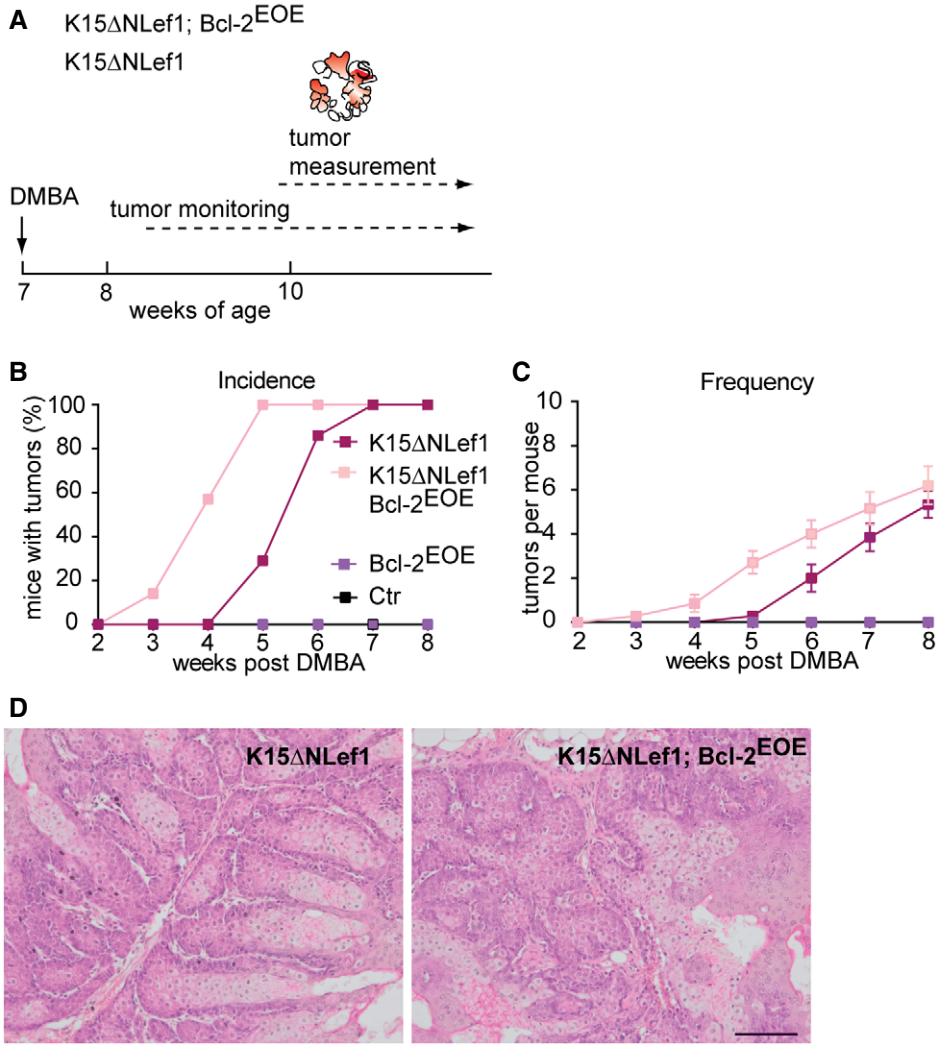

Figure 7. Bcl-2 promotes SC-driven tumour initiation.

A Schematic of tumour experiment timeline in K15ΔNLef1 genetic background.

B, C Tumour incidence (B) and frequency (C) in Ctr, Bcl-2^{EOE}, K15ΔNLef1 and K15ΔNLef1;Bcl-2^{EOE} mice (n = 10 biological replicates; mean ± standard error of mean [SEM]).

D Histology of sebaceous tumours of K15ΔNLef1 and K15ΔNLef1;Bcl-2^{EOE} mice. Scale bar, 100μm.

(Fig EV5A). Tumour studies, involving initiation of Bcl-2 expression and DMBA treatment (Fig EV5B), revealed an increase in tumour initiation and tumour frequency (Fig EV5C and D) similar to the tumour-promoting effect seen in K15ΔNLef1/Bcl-2^{EOE} mice (Fig 7B and C), demonstrating that Bcl-2 overexpression specifically in HF BSCs is sufficient to promote skin tumour formation.

Together, the tumour studies suggested that BSCs overexpressing Bcl-2 possess an advantage to survive and are potentially selected to give rise to tumours (Fig EV5E).

Discussion

Regenerating tissues, including the mammalian skin, require a tight control of cell death mechanisms to prevent the tissue from overgrowth or degeneration. This applies particularly to tissue SCs, the main cellular source driving regeneration and repair following injury (Rognoni & Watt, 2018). Here, we show that blocking Bcl-2 function, either by a systemic treatment with a highly selective Bcl-2 inhibitor (ABT-199) or by conditional ablation of Bcl-2 from the mouse epidermis, results in BSC-specific apoptosis. Moreover, the cell death following ABT-199 treatment is specific to a BSC subpopulation, sbBSCs, highlighting a functional heterogeneity within the BSC compartment. Our results demonstrate that HF SC pools differ in their apoptotic response and that only sbBSCs are more dependent on Bcl-2 (Fig EV1F). Differential regulation of anti-apoptotic proteins and distinct cell survival requirements have also been observed in subsets of dendritic cells (Carrington *et al*, 2015) and thus might constitute an important molecular mechanism of functional specification in heterogeneous cell compartments.

Our study also reveals the physiological relevance for Bcl-2-mediated protection of sbBSCs by showing that sbBSC depletion significantly impairs cyclic HF regeneration and delays anagen entry. This finding is in line with previous data showing that the first postnatal hair regeneration cycle is retarded in Bcl-2 null mice (Veis *et al*, 1993; Kamada *et al*, 1995; Yamamura *et al*, 1996). It also raises the question how Bcl-2-regulated cell death affects HF BSC function and HF regeneration? Abrupt loss of sbBSC following ABT-199 treatment might result in the disruption of the normal architecture of the BSC compartment and thus impact on the physiological function of BSC during telogen to anagen transition. The hypothesis that sbBSCs directly affect bBSCs via intra-bulge cellular crosstalk is also appealing, and the direct contribution of sbBSCs to hair follicle growth during anagen may also be an interesting possibility that could be tested in the future.

In addition, our data show that epidermal Bcl-2 overexpression blocks apoptosis during catagen, when mature anagen HFs retract to transit to the telogen phase. Based on previous elegant live-imaging studies capturing cell death in the basal epithelial layer of HFs (Mesa *et al*, 2015b), our experiments suggested that the enlarged HF bulge compartment in Bcl-2^{EOE} mice was generated by basal and outer root sheath HF keratinocytes that are normally lost during catagen. Remarkably, despite the Bcl-2-induced block in the apoptosis of keratinocytes, HFs are still capable to retract in catagen. This observation supports recent findings that dermal sheath contraction is the main driver of epithelial column regression and refutes the prevailing hypothesis of an apoptotic force inducing follicle regression (Heitman *et al*, 2020).

One immediate consequence of the block of apoptosis during catagen in the epidermis of Bcl-2^{EOE} mice is the formation of an enlarged BSC compartment and an abnormal HG shape that are associated with a delay in anagen entry. Several potential mechanisms could cause the transient inhibition in hair regrowth. One explanation is that an abnormal HG impairs its intrinsic response to activating signals produced by the underlying DP (Greco *et al*, 2009). Another possibility is that the abnormal BSC and HG niche impacts on the molecular DP-HG crosstalk that is essential for anagen initiation (Mesa *et al*, 2015a). Finally, Bcl-2 overexpression and apoptosis defects may lead to an enhanced quiescence in BSCs, a hypothesis that is supported by the elevated expression of quiescent SC markers, including Nfatc1 and FoxC1. In this case, the molecular signals activating hair growth may need to overcome a threshold that is higher in Bcl-2^{EOE} mice than under normal physiological conditions (Blanpain & Fuchs, 2006; Greco *et al*, 2009). Collectively, our *in vivo* studies of the gain and loss of function of Bcl-2 revealed that although cyclic HF renewal is disturbed by significantly delaying anagen in both experimental settings, the underlying cellular mechanisms are different. We identify Bcl-2 as a key molecule controlling BSC homeostasis and activity during HF regeneration, as well as regulating the architecture, size and composition of the SC pool.

Acquired resistance towards apoptosis is one of the hallmarks of cancer stem cells and often leads to the failure of anticancer treatment strategies (Hanahan & Weinberg, 2011). Given that Bcl-2 is intimately linked to diverse haematologic malignancies and is frequently abnormally regulated in many types of cancer (Brinkmann & Kashkar, 2014), we investigated the roles of Bcl-2 in BSC-driven tumour formation. Previous studies suggested that Bcl-2 overexpression leads to an increase in resistance of BSCs towards DNA damage-induced cell death following ionizing radiation of mouse skin, thereby safeguarding BSCs (Sotiropoulou *et al*, 2010). Our findings show that the epidermal tumours exhibit high levels of BCL-2 protein and that different levels of Bcl-2 influence tumour development in mice. Thus, we propose a model where SCs that have higher amounts of Bcl-2 protein are selected to give rise to tumours perhaps due to the accumulation of DNA damage (Sotiropoulou *et al*, 2010; Petersson *et al*, 2015) (Fig EV5E). Furthermore, our results suggest that treating skin tumours with the Bcl-2 inhibitor ABT-199 can potentially induce apoptosis of tumour cells, with promising clinical implications in the future. In agreement with this, a treatment regimen targeting Bcl-2 proteins led to a remarkable therapeutic success in haematologic malignancies (Thijssen & Roberts, 2019). However, alternative relapse mechanisms and patients suffering from secondary malignancies, including skin lesions (Solomon *et al*, 2016), highlight the necessity to better understand the potential role of Bcl-2 and apoptosis modalities in other tissues and cancers, such as skin cancer.

Materials and Methods

Experimental mice

K14Cre, K19CreER, Lgr5CreER-eGFP, Lrig1CreER-eGFP, K15ΔNLef1, Bcl-2^{flox}, and Rosa26$^{LSL.BCL2.IRES.GFP}$ mice have been described before (Hafner *et al*, 2004; Thorp *et al*, 2009; Petersson *et al*, 2011;

Knittel *et al*, 2016). K14Cre mice were crossed with Bcl-2^{flox} mice to generate Bcl-2 epidermal knockout mice (Bcl-2^{EKO}). To generate epidermal Bcl-2 overexpressing mice (Bcl-2^{EOE}), K14Cre mice were crossed with Rosa$26^{LSL.BCL2.IRES.GFP}$. Bcl-2^{EOE} mice were further crossed with K15ΔNLef1 mice. All mouse strains were maintained on a C57Bl/6 background. For all experiments, mice of the same sex were used. Mice were group-housed on a 12:12-h day (light) and night (dark) cycle in specific pathogen-free (SPF) cages. All *in vivo* experiments were carried out according to ethical guidelines and the animal licence given by the State Office North-Rhine Westphalia.

Inhibitor and tamoxifen treatment

ABT-199 (50 mg/kg) or the control solution was injected i.p. for one or six consecutive days into 7-week-old wild-type mice (Vaillant *et al*, 2013). For a stock solution, ABT-199 was dissolved in DMSO (50 mg/ml). 5% glucose, propylene glycol and Tween 20 (13:6:1) were added to generate working solution. For some experiments, mouse back skin was shaved following inhibitor treatment for 6 days using an electric shaver (Wella Contura) when mice were in the telogen phase. Hair-coat recovery was monitored once per day for up to 6 weeks. 7-week-old Bcl-2^{K19OE} mice, K15ΔNLef1; Bcl-2^{K19OE} mice and control littermates were i.p. injected with 2 mg tamoxifen for four consecutive days prior DMBA tumour experiments.

Tumour experiments

To initiate tumorigenesis, 7-week-old wild-type (n = 10), K15ΔNLef1 (n = 10), Bcl-2^{EOE} (n = 10), K15ΔNLef1; Bcl-2^{EOE} (n = 10), Bcl-2^{K19OE} mice ($n \geq 5$) and K15ΔNLef1; Bcl-2^{K19OE} mice ($n \geq 5$) were treated once with 650 μM 7,12-dimethylbenz(a)anthracene (DMBA; Sigma-Aldrich). 3–5 weeks later, tumour formation was observed. Tumours were monitored and scored once per week.

Isolation of epidermal whole mounts

Epidermal whole mounts of tail skin were isolated as described before (Braun *et al*, 2003). In brief, tail skin was incubated in 5 mM EDTA/PBS for 3 h at 37°C. Epidermis was gently peeled off using forceps and fixed in 3.4% formaldehyde for 1 h at RT and afterwards stored in PBS at 4°C.

Immunofluorescence and microscopy

Epidermal whole mounts and skin tissue sections were analysed by immunofluorescence according to established protocols. In brief, skin or tumour tissue was either directly embedded in OCT (Tissue Tek) and frozen or fixed in 4% formaldehyde and embedded in paraffin. Antibodies were diluted in blocking solution. The following primary antibodies were used: K15 (mouse, Neomarkers, 1:1,500), K14 (rabbit, Covance, 1:3,000), K10 (rabbit, Covance, 1:500), K6 (rabbit, Covance, 1:3,000), active Caspase 3 (rabbit, R&D Systems, 1:500), BrdU (mouse, BD Bioscience, 1:50), P-Cadherin (rat, Invitrogen, 1:400), Nfatc1 (7A6, mouse, DSHB), Sox9 (rabbit, Millipore, 1:1,000), Scd1 (rat, R&D, 1:100), BrdU (rat, Oxford Biotechnology, 1:500), K15 (rabbit, Progen, 1:1,500), Integrin α6 (rat, BD, 1:1,000), γH2AX (rabbit, Cell Signaling, 1:200), K71, K72, K75, K85 (guinea pig, Progen, ready-to-use kit), Bcl-2 (mouse, BD Bioscience, 1:200), Trp2 (goat, Santa Cruz, 1:200) and GFP-AlexaFITC (goat, Rockland, 1:500). All secondary antibodies coupled to Alexa488 and Alexa594 were obtained from Molecular Probes. Individual immunostainings were performed at least twice. Whole mount stainings were analysed using Olympus Fluoview FV1000 confocal microscope, and tissue sections were analysed using Olympus fluorescence microscope IX83 and IX81. Retracting epithelial strands were measured with Olympus cellSens Dimension software.

Flow cytometry

Skin was harvested, the fat tissue removed and then floated on 0.25 mg/ml thermolysin (Sigma) in PBS with the dermal side down for 45 min at 37°C. Epidermis and dermis were separated, and the epidermal tissue was minced, filtered and washed with 4% FCS, 2 mM EDTA/PBS. For SC quantification and sorting, cell suspensions were incubated in 4%FCS, 2 mM EDTA/PBS for 45 min at 4°C with the following antibodies: phycoerythrin (PE)-conjugated α6-integrin (CD49f, BD PharMingen; 1:25) and eFlour660-coupled CD34 (Ram34, eBioscience; 1:100). Cell viability was assessed by 7AAD (BD Bioscience) labelling. Subsequent analysis was carried out using a FACSCanto™II Cytometer (BD Bioscience) equipped with BD FACSDiva Software. Cell sorting for analysis and RNA sequencing of BSC subpopulations were performed on a FACSAria™ IIIu and FACSAria™Fusion cell sorters (BD Bioscience).

RNA sequencing

For RNA sequencing of the sorted BSC subpopulations, RNA from four mice per FACS sorted cell population ($CD34^-$, $CD34^+$/$Itga6^{High}$, $CD34^+$/$Itga6^{Low}$) was pooled. Due to low amount of input material, pre-amplification using the Ovation RNASeq System V2 was performed. Total RNA was used for first-stranded cDNA synthesis using both poly(T) and random primers, followed by second-stranded synthesis and isothermal strand-displacement amplification. For library preparation, the Illumina NextEra XT DNA sample preparation protocol was used with 1 ng cDNA input. After validation (Agilent 2200 TapeStation) and quantification (Invitrogen Qubit System), all transcriptome libraries were pooled. The pool was quantified using the Peqlab KAPA Library Quantification Kit and the Applied Biosystems 7900HT Sequence Detection and sequenced on an Illumina HiSeq4000 sequencing instrument with a 2 × 75 bp paired-end read length.

RNA-Seq data were processed through the QuickNGS pipeline according to Wagle *et al*, 2015 (Wagle *et al*, 2015) using Ensembl version 87(mm10). Reads were mapped to the Mouse genome using Tophat (version 2.0.12) and abundance estimation with Cufflinks (Version 2.1.1). DESeq2 was used for differential gene expression analysis. The results were uploaded into the QuickNGS database.

GO-term enrichment analysis was performed using the Metascape software using differentially expressed genes in sbBSCs compared to bBSCs as input (> 2-fold change, P-value > 0.05).

qRT–PCR analysis

Total RNA was isolated from epidermis, FAC-sorted bulge SCs and skin tumours, and qRT–PCR experiments were performed using primers (eurofins; Appendix Table S1).

The following TaqMan probes were used: Bcl-2, Mm00477631, NfatC1, Mm01265944 and 18S, Mm03928990 (Thermo Scientific).

The expression levels were calculated relative to 18S RNA using the ΔΔCT method (ΔΔCT = ΔCT 18S RNA − ΔCT gen of interest) (Schmittgen & Livak, 2008). The cycle threshold (CT) value is defined as the number of cycles required to overcome a threshold, which exceeds the background level.

Western blot analysis

Back skin epidermis or tumour samples were homogenized in crude lysis buffer (1% w/v SDS, 10 mM EDTA) with metal beads through the Minilys homogenizer (Bertin technologies). Total protein (25 μg) was loaded in Bolt™ 4–12%, Bis–Tris, 1.0 mm, Mini Protein Gel (Invitrogen). Proteins were then transferred to PVDF membranes. Primary and secondary antibodies were diluted in 5% milk in TBS-0.01% Tween buffer. The following primary antibodies were used: Bcl-2 (mouse, BD Bioscience, 1:500), K14 (rabbit, Covance, 1:3,000), Scd1 (rat, R&D, 1:500), GAPDH (rabbit, Cell Signaling, 1:2,000) and α-actinin (rabbit, Cell Signaling, 1:1,000). All secondary antibodies coupled to HRP were obtained from GE Healthcare. WESTAR ECL Substrate for Western blotting (Cyanagen) was used to visualize the bands.

Statistical analysis

Statistical significance was calculated using Student's *t*-test, except for analysing differences in tumour frequency. Statistical analysis of differences in tumour frequency was carried out using two-way ANOVA with repeated measures. Quantification methods are indicated in the respective Figure legends. All *P*-values below 0.05 were considered significant. Statistical analyses were performed using Microsoft Excel and GraphPad Prism.

Data availability

The data sets produced in this study are available in the following database: Gene Expression Omnibus GSE166921 (https://www.ncbi.nlm.nih.gov/geo/query/acc.cgi?acc=GSE166921).

Expanded View for this article is available online.

Acknowledgements
We thank H. Bazzi and T. Krieg for discussions and comments on the manuscript. We thank C. Blanpain for sharing data and M. Kasper, K. Annusver, N. Peltzer, L. Frenzel, A. da Palma Guerreiro and K. Ellsworth for experimental support and discussion. Experiments were supported through Center for Molecular Medicine Cologne (CMMC) core facilities (Animal facility, Cell sorting, Tissue embedding and Microscopy), MPI for Biology of Ageing FACS & Imaging facility, Animal facility at the Department of Pharmacology, CECAD Bioinformatics facility and the Cologne Center for Genomics (CCG) of the University of Cologne. The project was funded by the Deutsche Forschungsgemeinschaft (DFG, German Research Foundation)—Project-ID 73111208—SFB 829 and a CMMC project grant to C.N. A.G. and G.M. were supported by a CMMC project grant and Köln Fortune funding by the Medical Faculty of the University of Cologne. H.K. received funding from the CRC 1218 (Project-ID 269925409) and CRC 1403 (Project-ID 414786233). Open Access funding enabled and organized by Projekt DEAL.

Author contributions
AG, GM and CN designed the experiments. CN wrote the manuscript. AG, GM and FK performed experiments and PS and MN assisted with expression and tissue analysis. JMS and HK generated and analysed Rosa26$^{LSL.BCL2.IRES.GFP}$ mice. All authors discussed the data and participated in the manuscript preparation and editing. CN supervised the study.

Conflict of interest
The authors declare that they have no conflict of interest.

References

Blanpain C, Lowry WE, Geoghegan A, Polak L, Fuchs E (2004) Self-renewal, multipotency, and the existence of two cell populations within an epithelial stem cell niche. *Cell* 118: 635 – 648

Blanpain C, Fuchs E (2006) Epidermal stem cells of the skin. *Annu Rev Cell Dev Biol* 22: 339 – 373

Braun KM, Niemann C, Jensen UB, Sundberg JP, Silva-Vargas V, Watt FM (2003) Manipulation of stem cell proliferation and lineage commitment: visualisation of label-retaining cells in wholemounts of mouse epidermis. *Development* 130: 5241 – 5255

Brinkmann K, Kashkar H (2014) Targeting the mitochondrial apoptotic pathway: a preferred approach in hematologic malignancies? *Cell Death Dis* 5: e1098

Carrington EM, Zhang JG, Sutherland RM, Vikstrom IB, Brady JL, Soo P, Vremec D, Allison C, Lee EF, Fairlie WD *et al* (2015) Prosurvival Bcl-2 family members reveal a distinct apoptotic identity between conventional and plasmacytoid dendritic cells. *Proc Natl Acad Sci USA* 112: 4044 – 4049

Cotsarelis G, Sun TT, Lavker RM (1990) Label-retaining cells reside in the bulge area of pilosebaceous unit: implications for follicular stem cells, hair cycle, and skin carcinogenesis. *Cell* 61: 1329 – 1337

Debrincat MA, Pleines I, Lebois M, Lane RM, Holmes Ml, Corbin J, Vandenberg CJ, Alexander WS, Ng AP, Strasser A *et al* (2015) BCL-2 is dispensable for thrombopoiesis and platelet survival. *Cell Death Dis* 6: e1721

Donati G, Watt FM (2015) Stem cell heterogeneity and plasticity in epithelia. *Cell Stem Cell* 16: 465 – 476

Duverger O, Morasso MI (2009) Epidermal patterning and induction of different hair types during mouse embryonic development. *Birth Defects Res C Embryo Today* 87: 263 – 272

Frances D, Sharma N, Pofahl R, Maneck M, Behrendt K, Reuter K, Krieg T, Klein CA, Haase I, Niemann C (2015) A role for Rac1 activity in malignant progression of sebaceous skin tumors. *Oncogene* 34: 5505 – 5512

Galluzzi L, Vitale I, Aaronson SA, Abrams JM, Adam D, Agostinis P, Alnemri ES, Altucci L, Amelio I, Andrews DW *et al* (2018) Molecular mechanisms of cell death: recommendations of the Nomenclature Committee on Cell Death 2018. *Cell Death Differ* 25: 486 – 541

Ganzel C, Ram R, Gural A, Wolach O, Gino-Moor S, Vainstein V, Nachmias B, Apel A, Koren-Michowitz M, Pasvolsky O *et al* (2020) Venetoclax is safe and efficacious in relapsed/refractory AML. *Leuk Lymphoma* 61: 2221 – 2225

Greco V, Chen T, Rendl M, Schober M, Pasolli HA, Stokes N, Dela Cruz-Racelis J, Fuchs E (2009) A two-step mechanism for stem cell activation during hair regeneration. *Cell Stem Cell* 4: 155 – 169

Hafner M, Wenk J, Nenci A, Pasparakis M, Scharffetter-Kochanek K, Smyth N, Peters T, Kess D, Holtkötter O, Shephard P *et al* (2004) Keratin 14 Cre transgenic mice authenticate keratin 14 as an oocyte-expressed protein. *Genesis* 38: 176 – 181

Hanahan D, Weinberg RA (2011) Hallmarks of cancer: the next generation. *Cell* 144: 646 – 674

Heitman N, Sennett R, Mok K-W, Saxena N, Srivastava D, Martino P, Grisanti L, Wang Z, Ma'ayan A, Rompolas P *et al* (2020) Dermal sheath contraction powers stem cell niche relocation during hair cycle regression. *Science* 367: 161 – 166

Hoi CS, Lee SE, Lu SY, McDermitt DJ, Osorio KM, Piskun CM, Peters RM, Paus R, Tumbar T (2010) Runx1 directly promotes proliferation of hair follicle stem cells and epithelial tumor formation in mouse skin. *Mol Cell Biol* 30: 2518 – 2536

Horsley V, Aliprantis AO, Polak L, Glimcher LH, Fuchs E (2008) NFATc1 balances quiescence and proliferation of skin stem cells. *Cell* 132: 299 – 310

Hsu YC, Pasolli HA, Fuchs E (2011) Dynamics between stem cells, niche, and progeny in the hair follicle. *Cell* 144: 92 – 105

Joost S, Zeisel A, Jacob T, Sun X, La Manno G, Lonnerberg P, Linnarsson S, Kasper M (2016) Single-cell transcriptomics reveals that differentiation and spatial signatures shape epidermal and hair follicle heterogeneity. *Cell Syst* 3: 221 – 237.e229

Kamada S, Shimono A, Shinto Y, Tsujimura T, Takahashi T, Noda T, Kitamura Y, Kondoh H, Tsujimoto Y (1995) bcl-2 deficiency in mice leads to pleiotropic abnormalities: accelerated lymphoid cell death in thymus and spleen, polycystic kidney, hair hypopigmentation, and distorted small intestine. *Cancer Res* 55: 354 – 359

Kimura-Ueki M, Oda Y, Oki J, Komi-Kuramochi A, Honda E, Asada M, Suzuki M, Imamura T (2012) Hair cycle resting phase is regulated by cyclic epithelial FGF18 signaling. *J Invest Dermatol* 132: 1338 – 1345

Kishimoto J, Burgeson RE, Morgan BA (2000) Wnt signaling maintains the hair-inducing activity of the dermal papilla. *Genes Dev* 14: 1181 – 1185

Knittel G, Liedgens P, Korovkina D, Seeger JM, Al-Baldawi Y, Al-Maarri M, Fritz C, Vlantis K, Bezhanova S, Scheel AH *et al* (2016) B-cell-specific conditional expression of Myd88p.L252P leads to the development of diffuse large B-cell lymphoma in mice. *Blood* 127: 2732 – 2741

Lavker RM, Sun T-T, Oshima H, Barrandon Y, Akiyama M, Ferraris C, Chevalier G, Favier B, Jahoda CAB, Dhouailly D *et al* (2003) Hair follicle stem cells. *J Investig Dermatol Symp Proc* 8: 28 – 38

Leishman E, Howard JM, Garcia GE, Miao Q, Ku AT, Dekker JD, Tucker H, Nguyen H (2013) Foxp1 maintains hair follicle stem cell quiescence through regulation of Fgf18. *Development* 140: 3809 – 3818

Lindner G, Botchkarev VA, Botchkareva NV, Ling G, van der Veen C, Paus R (1997) Analysis of apoptosis during hair follicle regression (catagen). *Am J Pathol* 151: 1601 – 1617

Liu Y, Lyle S, Yang Z, Cotsarelis G (2003) Keratin 15 promoter targets putative epithelial stem cells in the hair follicle bulge. *J Invest Dermatol* 121: 963 – 968

Mak SS, Moriyama M, Nishioka E, Osawa M, Nishikawa S (2006) Indispensable role of Bcl2 in the development of the melanocyte stem cell. *Dev Biol* 291: 144 – 153

Mason KD, Carpinelli MR, Fletcher JI, Collinge JE, Hilton AA, Ellis S, Kelly PN, Ekert PG, Metcalf D, Roberts AW *et al* (2007) Programmed anuclear cell death delimits platelet life span. *Cell* 128: 1173 – 1186

Means AL, Xu Y, Zhao A, Ray KC, Gu G (2008) A CK19(CreERT) knockin mouse line allows for conditional DNA recombination in epithelial cells in multiple endodermal organs. *Genesis* 46: 318 – 323

Merrill BJ, Gat U, DasGupta R, Fuchs E (2001) Tcf3 and Lef1 regulate lineage differentiation of multipotent stem cells in skin. *Genes Dev* 15: 1688 – 1705

Mesa KR, Rompolas P, Greco V (2015a) The dynamic duo: niche/stem cell interdependency. *Stem Cell Rep* 4: 961 – 966

Mesa KR, Rompolas P, Zito G, Myung P, Sun TY, Brown S, Gonzalez DG, Blagoev KB, Haberman AM, Greco V (2015b) Niche-induced cell death and epithelial phagocytosis regulate hair follicle stem cell pool. *Nature* 522: 94 – 97

Morrison SJ, Scadden DT (2014) The bone marrow niche for haematopoietic stem cells. *Nature* 505: 327 – 334

Müller-Röver S, Rossiter H, Lindner G, Peters EMJ, Kupper TS, Paus R (1999) Hair follicle apoptosis and Bcl-2. *J Investig Dermatol Symp Proc* 4: 272 – 277

Niemann C, Owens DM, Schettina P, Watt FM (2007) Dual role of inactivating Lef1 mutations in epidermis: tumor promotion and specification of tumor type. *Cancer Res* 67: 2916 – 2921

Nowak JA, Polak L, Pasolli HA, Fuchs E (2008) Hair follicle stem cells are specified and function in early skin morphogenesis. *Cell Stem Cell* 3: 33 – 43

Paus R, Cotsarelis G (1999) The biology of hair follicles. *N Engl J Med* 341: 491 – 497

Petersson M, Brylka H, Kraus A, John S, Rappl G, Schettina P, Niemann C (2011) TCF/Lef1 activity controls establishment of diverse stem and progenitor cell compartments in mouse epidermis. *EMBO J* 30: 3004 – 3018

Petersson M, Reuter K, Brylka H, Kraus A, Schettina P, Niemann C (2015) Interfering with stem cell-specific gatekeeper functions controls tumour initiation and malignant progression of skin tumours. *Nat Commun* 6: 5874

Puthalakath H, Villunger A, O'Reilly LA, Beaumont JG, Coultas L, Cheney RE, Huang DC, Strasser A (2001) Bmf: a proapoptotic BH3-only protein regulated by interaction with the myosin V actin motor complex, activated by anoikis. *Science* 293: 1829 – 1832

Rendl M, Polak L, Fuchs E (2008) BMP signaling in dermal papilla cells is required for their hair follicle-inductive properties. *Genes Dev* 22: 543 – 557

Rognoni E, Watt FM (2018) Skin cell heterogeneity in development, wound healing, and cancer. *Trends Cell Biol* 28: 709 – 722

Rompolas P, Greco V (2014) Stem cell dynamics in the hair follicle niche. *Semin Cell Dev Biol* 25–26: 34 – 42

Schmittgen TD, Livak KJ (2008) Analyzing real-time PCR data by the comparative CT method. *Nat Protoc* 3: 1101 – 1108

Solomon BM, Chaffee KG, Moreira J, Schwager SM, Cerhan JR, Call TG, Kay NE, Slager SL, Shanafelt TD (2016) Risk of non-hematologic cancer in individuals with high-count monoclonal B-cell lymphocytosis. *Leukemia* 30: 331 – 336

Sotiropoulou PA, Candi A, Mascré G, De Clercq S, Youssef KK, Lapouge G, Dahl E, Semeraro C, Denecker G, Marine J-C *et al* (2010) Bcl-2 and accelerated DNA repair mediates resistance of hair follicle bulge stem cells to DNA-damage-induced cell death. *Nat Cell Biol* 12: 572 – 582

Souers AJ, Leverson JD, Boghaert ER, Ackler SL, Catron ND, Chen J, Dayton BD, Ding H, Enschede SH, Fairbrother WJ *et al* (2013) ABT-199, a potent and selective BCL-2 inhibitor, achieves antitumor activity while sparing platelets. *Nat Med* 19: 202 – 208

Taddei ML, Giannoni E, Fiaschi T, Chiarugi P (2012) Anoikis: an emerging hallmark in health and diseases. *J Pathol* 226: 380 – 393

Taylor RC, Cullen SP, Martin SJ (2008) Apoptosis: controlled demolition at the cellular level. *Nat Rev Mol Cell Biol* 9: 231 – 241

Thijssen R, Roberts AW (2019) Venetoclax in lymphoid malignancies: new insights, more to learn. *Cancer Cell* 36: 341 – 343

Thorp E, Li Y, Bao L, Yao PM, Kuriakose G, Rong J, Fisher EA, Tabas I (2009) Brief report: increased apoptosis in advanced atherosclerotic lesions of Apoe-/- mice lacking macrophage Bcl-2. *Arterioscler Thromb Vasc Biol* 29: 169 – 172

Vaillant F, Merino D, Lee L, Breslin K, Pal B, Ritchie M, Smyth G, Christie M, Phillipson L, Burns C *et al* (2013) Targeting BCL-2 with the BH3 mimetic ABT-199 in estrogen receptor-positive breast cancer. *Cancer Cell* 24: 120 – 129

Vandenberg CJ, Cory S (2013) ABT-199, a new Bcl-2-specific BH3 mimetic, has *in vivo* efficacy against aggressive Myc-driven mouse lymphomas without provoking thrombocytopenia. *Blood* 121: 2285 – 2288

Veis DJ, Sorenson CM, Shutter JR, Korsmeyer SJ (1993) Bcl-2-deficient mice demonstrate fulminant lymphoid apoptosis, polycystic kidneys, and hypopigmented hair. *Cell* 75: 229 – 240

Vidal VP, Chaboissier MC, Lutzkendorf S, Cotsarelis G, Mill P, Hui CC, Ortonne N, Ortonne JP, Schedl A (2005) Sox9 is essential for outer root sheath differentiation and the formation of the hair stem cell compartment. *Curr Biol* 15: 1340 – 1351

Vogler M, Dinsdale D, Dyer MJ, Cohen GM (2013) ABT-199 selectively inhibits BCL2 but not BCL2L1 and efficiently induces apoptosis of chronic lymphocytic leukaemic cells but not platelets. *Br J Haematol* 163: 139 – 142

Wagle P, Nikolic M, Frommolt P (2015) QuickNGS elevates next-generation sequencing data analysis to a new level of automation. *BMC Genom* 16: 487

Woo WM, Zhen HH, Oro AE (2012) Shh maintains dermal papilla identity and hair morphogenesis via a Noggin-Shh regulatory loop. *Genes Dev* 26: 1235 – 1246

Yamamura K, Kamada S, Ito S, Nakagawa K, Ichihashi M, Tsujimoto Y (1996) Accelerated disappearance of melanocytes in bcl-2-deficient mice. *Cancer Res* 56: 3546 – 3550

Yu P, Nie Q, Tang C, Zhang L (2018) Nanog induced intermediate state in regulating stem cell differentiation and reprogramming. *BMC Syst Biol* 12: 22

Zhou Y, Zhou B, Pache L, Chang M, Khodabakhshi AH, Tanaseichuk O, Benner C, Chanda SK (2019) Metascape provides a biologist-oriented resource for the analysis of systems-level datasets. *Nat Commun* 10: 1523